Multi-Objective Optimal Model Predictive Control for Three-Level ANPC Grid-Connected Inverter

Xia, Zhenglong; Liu, Zhan; Guerrero, Josep M.

Published in:
IEEE Access

DOI (link to publication from Publisher):
10.1109/ACCESS.2020.2981996

Publication date:
2020

Document Version
Publisher's PDF, also known as Version of record

IEEE Access
Multidisciplinary | Rapid Review | Open Access Journal

Received March 2, 2020, accepted March 17, 2020, date of publication March 19, 2020, date of current version April 7, 2020.

Digital Object Identifier 10.1109/ACCESS.2020.2981996

Multi-Objective Optimal Model Predictive Control for Three-Level ANPC Grid-Connected Inverter

ZHENGLONG XIA[1], (Member, IEEE), ZHAN LIU[1], (Member, IEEE), AND JOSEP M. GUERRERO[2], (Fellow, IEEE)

[1]School of Electrical Engineering and Automation, Jiangsu Normal University, Xuzhou 221116, China
[2]Center for Research on Microgrids (CROM), Department of Energy Technology, Aalborg University, 9220 Aalborg East, Denmark

Corresponding author: Zhan Liu (liuzhan@jsnu.edu.cn)

This work was supported by the Youth Fund of the Foundation Research Project of Jiangsu Province under Grant BK20160219, the National Natural Science Foundation of China under Grant 51907083 and J. M. Guerrero was funded by a Villum Investigator under Grant 25920 from The Villum Fonden.

ABSTRACT The three-level active-neutral-point-clamped (ANPC) grid-connected inverter is a promising alternative for photovoltaic (PV) power generation, thanks to its capability of balancing the losses of power devices. This paper proposes a multi-objective optimal model predictive control (MO^2-MPC) algorithm for three-level ANPC grid-connected inverter, and thus the number of rolling optimizations of the model can be reduced by eliminating the switching states of the three-level output that violate the unit level jump principle. The power loss of each switch was calculated in real time by the linear fitting of the turn-on and turn-off losses of the switches, and the imbalanced losses were added to the target cost function to minimize imbalance losses. Finally, the proposed control method was proved correct and effective through an experiments prototype.

INDEX TERMS Three-level active-neutral-point-clamped (3L-ANPC), grid-connected inverter, multi-objective optimal model predictive control (MO^2-MPC), balancing the losses of power switches.

I. INTRODUCTION

The world is witnessing an energy reform driven by environmental and resource constraints. Many concrete efforts have been paid to implement the reform, including building smart grids, setting up an energy Internet, and developing low-carbon renewable energies [1]–[8]. Photovoltaic (PV) power and wind power are two popular kinds of such energies [9]. In the PV and wind power generation systems, the three-level active-neutral-point-clamped (ANPC) grid-connected inverter can output more zero-switching states than the traditional three-level diode-clamped inverter, thus balancing the power losses of power switches in the bridge arm and maximizing the power output of grid-connected inverter become possible [10], [11].

The predictive control has received extensive attention in the field of power electronic converters, since the predictive control theory on the finite control set model was successfully applied to two-level inverter by Chilean scholar Jose Rodriguez in 2007 [12]. The model predictive control (MPC) gains many advantages in regulating the power of three-level ANPC grid-connected inverter, such as fast power response and multi-target optimization [13]. The feasibility of using MPC to achieve multi-objective optimization is verified theoretically [14]. When the MPC is adopted for multi-level inverter, however, both the number of rolling optimizations and computing time will increase at an exponential rate N3 with the number of switching states. In this case, the traditional predictive control cannot achieve satisfactory results [15]. To solve the problem, reference [16] details the effects of levels with different topologies and their switching states on online optimization. Based on the optimal spatial vector position for tracking error elimination, reference [17] develops a control strategy for selecting the feasible switching states. The strategy can reduced the number of rolling optimizations for switching states and improve the optimization efficiency, but it is hard to implement. Reference [18] designs an offline controller capable of predictive control, which avoids the excessive computing load of online MPC.

However, the controller cannot realize accurate offline segmentation due to the huge data storage. Considering the unbalanced power losses of power switches in three-level neutral-point-clamped (NPC) grid-connected inverter, References [19] advises to balance the losses of power switches

The associate editor coordinating the review of this manuscript and approving it for publication was Derek Abbott.

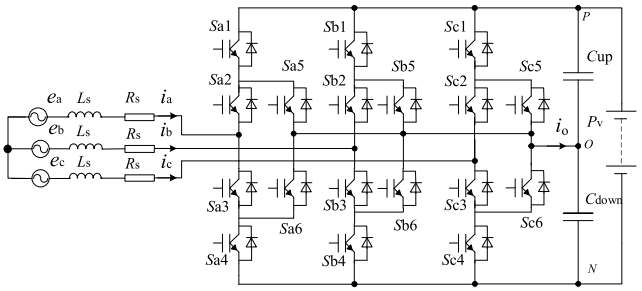

FIGURE 1. The topological structure of three-level ANPC grid-connected inverter.

and elevate the maximum output power of the system by replacing the traditional three-level NPC inverter with three-level ANPC inverter.

References [20] gives a loss calculation method based on linear fitting, which can compute the switching loss of each device in real-time; nonetheless, the calculated loss deviates greatly from the actual value, because the voltage across the switch tube and the current through the power switches in a switch cycle are changing. References [21], [22] propose a method to complete the switching loss using the exponential power function. Reference [23] presents a loss calculation method based on the power switches model, yet the method requires repeated iterations, making it unsuitable for online real-time calculation.

Targeting the three-level ANPC inverter, this paper puts forward a multi-objective optimal model predictive control (MO^2-MPC) algorithm. Compared with the traditional predictive control, the MO^2-MPC requires a few number of rolling optimizations in model prediction, consumes a short time through the predictive control, and considers the power losses of power switches in the target cost function. Then, the proposed control method was verified through simulation and experiment. The results show that the MO^2-MPC can balance the losses of power switches in three-level ANPC grid-connected inverter, and enhance the output power of the device.

II. THE PRINCIPLE OF THREE-LEVEL ANPC GRID-CONNECTED INVERTER AND THE ESTABLISHMENT OF PREDICTION MODEL FOR TRADITIONAL TARGETS

The topological structure of three-level ANPC grid-connected inverter is displayed in Fig.1, where e_a, e_b and e_c are the AC grid-side voltages; L_s is the inductance of the three-phase incoming line; R_s is the grid-side stray resistance; U_{up} and U_{down} are the voltages of the upper and lower buses, respectively.

Tab.1 lists the switching states of three-level ANPC grid-connected inverter. It can be seen that there are three more groups of switching states in ANPC inverter than the traditional NPC inverter, when the output level is zero.

Fig.2 shows the switching diagram of different switching states of three-level ANPC grid-connected inverter, the solid line in the figure represents two switching states that can be switched to each other, then the dotted line represents

TABLE 1. Switching states of ANPC three-level rectifier.

Level	State	S_{x1}	S_{x2}	S_{x3}	S_{x4}	S_{x5}	S_{x6}	u_o
+1	P	1	1	0	0	0	1	u_{up}
0	OU1	0	1	0	0	1	0	0
0	OU2	0	1	0	1	1	0	0
0	OL1	0	0	1	0	0	1	0
0	OL2	1	0	1	0	0	1	0
-1	N	0	0	1	1	1	0	u_{down}

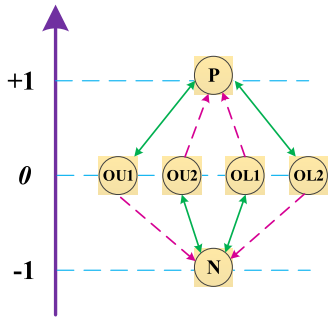

FIGURE 2. Switching diagram of different switching states of three-level ANPC grid-connected inverter.

the switching of the state and can only be switched in the direction of the arrow. The reason why the state P cannot be directly switched to the state OU2 is that the conduction of the switch S_{x4} has no effect on the equalization switching loss. At the same time, the reason that state P cannot be directly switched to state OL1 is that switching to state OL1 increases the loss of switch S_{x1} compared to directly switching to state OL2.

Under the ideal three-phase grid condition, the voltage in the two-phase stationary $\alpha\beta$ coordinate system can be expressed as:

$$L_s \frac{di_{\alpha,\beta}}{dt} = e_{\alpha,\beta} - u_{\alpha,\beta} - R_s i_{\alpha,\beta} \tag{1}$$

where L_s and R_s are the AC-side inductance and the grid-side stray resistance of the grid-connected inverter, respectively; $e_{\alpha,\beta}$ is the component of the grid voltage in the $\alpha\beta$ coordinate system; $u_{\alpha,\beta}$ is the component of the AC-side voltage of the grid-connected inverter in the $\alpha\beta$ coordinate system; $i_{\alpha,\beta}$ is the component of the grid-side current in the $\alpha\beta$ coordinate system.

Define the neutral point potential deviation as $u_o = u_{up}$-u_{down}. Then, the switch state of the output voltage of the neutral point potential can be described as:

$$\frac{du_o}{dt} = \frac{1}{2C}(i_\alpha |s_\alpha| + i_\beta |s_\beta|) \tag{2}$$

where C is the DC-side half-bus capacitance ($C = C_{up} = C_{down}$); s_α, s_β is the component of the switching states of the three-phase outputs from the grid-connected inverter in the $\alpha\beta$ coordinate system.

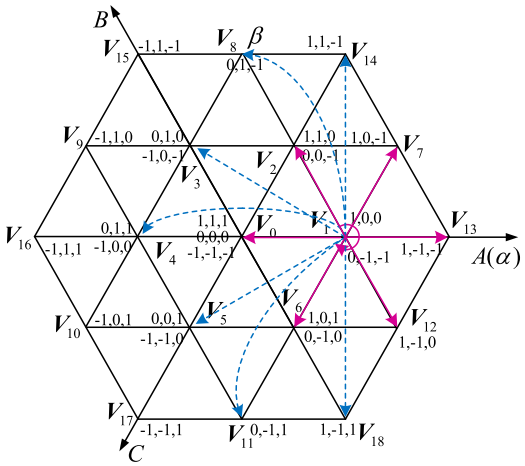

FIGURE 3. Level state optimization of three-level grid-connected inverter.

Assuming that the microprocessor samples at an interval of T_s, the following equations can be derived through the discretization of the differential terms of equations (1) and (2) according to the forward difference method:

$$\frac{di_{\alpha,\beta}}{dt} = \frac{i_{\alpha,\beta}(k) - i_{\alpha,\beta}(k-1)}{T_s} \tag{3}$$

$$\frac{du_o}{dt} = \frac{u_o(k) - u_o(k-1)}{T_s} \tag{4}$$

where k is the serial number of sampling in the system. Without considering the effect of stray resistance, the predicted value of $i_{\alpha,\beta}(k+1)$ can be deduced by substituting equation (3) into equation (1) and computing the last extrapolate:

$$i_{\alpha,\beta}(k+1) = i_{\alpha,\beta}(k) + \frac{\left[e_{\alpha,\beta}(k+1) - u_{\alpha,\beta}(k+1)\right] T_s}{L_s} \tag{5}$$

where $e_{\alpha,\beta}(k+1)$ is the component of the grid voltage in the $\alpha\beta$ coordinate system. Then, the $e_{\alpha,\beta}(k+1)$ can be predicted online by second-order extrapolation, which effectively reduces the delay of the digital control system:

$$e^*_{\alpha,\beta}(k+1) = 3e^*_{\alpha,\beta}(k) - 3e^*_{\alpha,\beta}(k-1) + e^*_{\alpha,\beta}(k-2) \tag{6}$$

Similarly, the prediction model for three-level neutral point potential discretization can be obtained from equations (2) and (4):

$$u_o(k+1) = u_o(k) + \frac{T_s}{2C}[i_\alpha(k+1)|s_\alpha(k+1)| + i_\beta(k+1)|s_\beta(k+1)|] \tag{7}$$

III. MO²-MPC PRINCIPLES OF THREE-LEVEL ANPC GRID-CONNECTED INVERTER

A. ROLLING OPTIMIZATION CONTROL OF THREE-LEVEL ANPC GRID-CONNECTED INVERTER

The MO²-MPC for three-level ANPC grid-connected inverter is modified from the traditional MPC-based direct power control: (1) The second-order extrapolation is adopted to predict the grid voltage online, which effectively reduces the delay of the digital control system; (2) The rolling of the system prediction model was optimized by removing some level states that deteriorate the performance of the grid-connected inverter before the model rolls, thus eliminating some unnecessary rolling calculations. The optimization of the level state of three-level grid-connected inverter is illustrated in Fig.3, where the dotted line and solid line respectively mean the level switching state is ineffective and effective.

The selection method can be detailed as: If the level states of the three-phase outputs are $S_a(k+1)$, $S_b(k+1)$ and $S_c(k+1)$, respectively, then the change of the line voltage level of the grid-connected inverter output, denoted respectively as $S_{jab}(k+1)$, $S_{jbc}(k+1)$ and $S_{jca}(k+1)$, the values of them can be obtained as:

$$\begin{cases} \text{abs}(S_a(k+1) - S_a(k)) \le 1 \\ \text{abs}(S_b(k+1) - S_b(k)) \le 1 \\ \text{abs}(S_c(k+1) - S_c(k)) \le 1 \\ -1 \le S_a(k+1) \le 1 \\ -1 \le S_b(k+1) \le 1 \\ -1 \le S_c(k+1) \le 1 \end{cases} \tag{8}$$

where abs() is the absolute cost function.

$$\begin{cases} S_{ab}(k+1) = S_a(k+1) - S_b(k+1) \\ S_{bc}(k+1) = S_b(k+1) - S_c(k+1) \\ S_{ca}(k+1) = S_c(k+1) - S_a(k+1) \\ -1 \le S_{ab}(k+1) \le 1 \\ -1 \le S_{bc}(k+1) \le 1 \\ -1 \le S_{ca}(k+1) \le 1 \end{cases} \tag{9}$$

If one of $S_{jab}(k+1)$, $S_{jbc}(k+1)$ and $S_{jca}(k+1)$ is greater than 2 in amplitude, this level state would be abandoned in the rolling optimization of the model.

Taking the current level state (0, 0, 0) for example, the number of rolling optimizations is reduced from 3^3=27 to 15 after the abandonment. The number of rolling is nearly halved, so the runtime of the processer will be greatly reduced. The rolling optimization control of three-level grid-connected inverter is described in Fig.4.

B. POWER SWITCH LOSSES BALANCING OF THREE-LEVEL ANPC GRID-CONNECTED INVERTER

The relationship between the energy generated from turn-on and turn-off and the collector current is fitted using the parameters of a certain type of insulated-gate bipolar transistor (IGBT), and plotted as Fig.5.

The fitting equation can be obtained as

$$\begin{cases} E_{on} = k^1_{on} i_c^3 + k^2_{on} i_c^2 + k^3_{on} i_c^1 + k^4_{on} \\ E_{off} = k^1_{off} i_c^3 + k^2_{off} i_c^2 + k^3_{off} i_c^1 + k^4_{off} \end{cases} \tag{10}$$

where $k^1_{on} = 3.35 \times 10^{-6}$; $k^2_{on} = 3.5 \times 10^{-3}$; $k^3_{on} = 0.7484$; $k^4_{on} = -0.6031$; $k^1_{off} = 2.51 \times 10^{-6}$; $k^2_{off} = 2.7 \times 10^{-3}$; $k^3_{off} = 0.5613$; $k^4_{off} = -0.4524$.

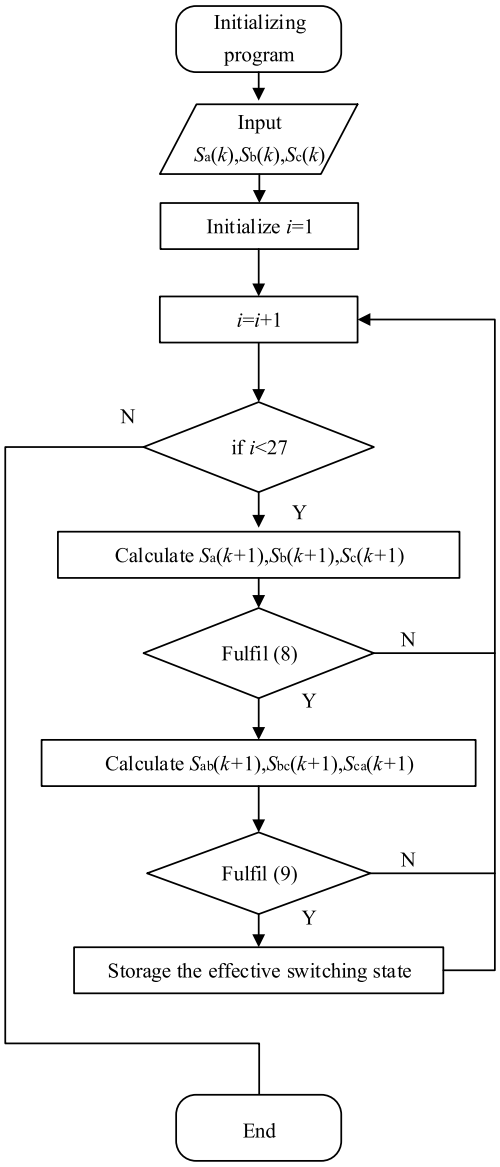

FIGURE 4. The flow chart for the rolling optimization control of three-level grid-connected inverter.

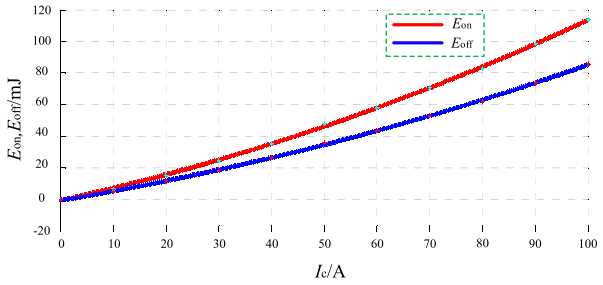

FIGURE 5. The fitting curve of IGBT losses.

Taking phase A switch tube S_{a1} as an example, the mean switching loss can be calculated as:

$$\overline{P}_{sw}(k+1) = f_{Fre}(E^i_{on} + E^i_{off}) \tag{11}$$

where f_{Fre} is the switching frequency of S_{a1}.

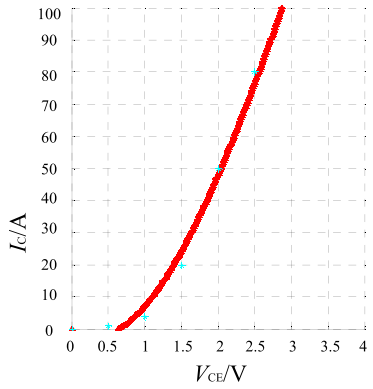

FIGURE 6. The fitting curve of IGBT output characteristics.

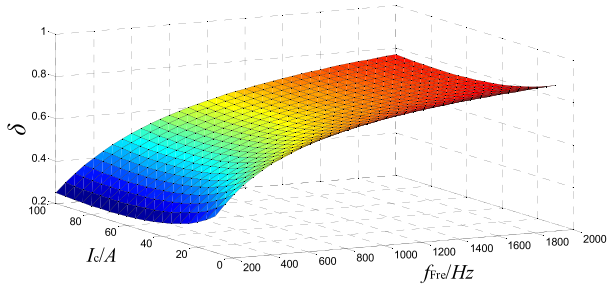

FIGURE 7. The three dimensions image of the ratio of switching loss.

In order to verify the conduction losses, the relationship between conduction voltage and conduction current is fitted out according to the parameters of IGBT output characteristics, and plotted as Fig.6.

According to the fitting curve, the power calculation formula of the conduction losses can be obtained as:

$$\overline{P}_{con} = V_{CE} \cdot \overline{I}_c = k^1_c \overline{I}^3_c + k^2_c \overline{I}^2_c + k^3_c \overline{I}_c \tag{12}$$

where $k^1_c = 2 \times 10^{-4}$; $k^2_c = 3.87 \times 10^{-2}$; $k^3_c = 0.49$

The mean power loss can be calculated as:

$$\overline{P}_{S_{a1}}(k+1) = \overline{P}_{SW}(k+1) + \overline{P}_{con}(k+1) \tag{13}$$

The proportion of switching loss of switch tube is defined by δ:

$$\delta = \overline{P}_{sw}/\overline{P}_{S_{a1}} \tag{14}$$

Fig.7 shows the three dimensions image of δ. It can be seen that with the increase of switching frequency, the switching loss is also increased, and the ratio of switching loss above 1 KHz is more than 60%. Therefore, if the switching frequency is reduced below 1 KHz, the switching loss will be greatly reduced.

The mean switching loss of three-level ANPC grid-connected inverter can be computed by:

$$P^-_s(k+1) = \frac{\sum_{i=1}^{6} (P_{S_{ai}}(k+1) + P_{S_{bi}}(k+1) + P_{S_{ci}}(k+1))}{18} \tag{15}$$

The root-mean-square power loss can be obtained as:

$$P_s(k+1)=\sqrt{\sum_{i=1}^{6}\begin{array}{l}((P_{Sai}(k+1)-P_s^-(k+1))^2\\+(P_{Sbi}(k+1)-P_s^-(k+1))^2\\+(P_{Sci}(k+1)-P_s^-(k+1))^2)\end{array}} \quad (16)$$

C. DIRECT POWER CONTROL OF THREE-LEVEL ANPC GRID-CONNECTED INVERTER BASED ON MO²-MPC

In the two-phase stationary $\alpha\beta$ coordinate system, the instantaneous power of three-level grid-connected inverter can be expressed as:

$$\begin{cases}P(k+1)=e_\alpha(k+1)i_\alpha(k+1)+e_\beta(k+1)i_\beta(k+1)\\Q(k+1)=e_\beta(k+1)i_\alpha(k+1)-e_\alpha(k+1)i_\beta(k+1)\end{cases} \quad (17)$$

where $P(k+1)$ and $Q(k+1)$ are the predicted values of the system. Then, the target cost function of three-level grid-connected inverter can be established according to the pre-set and actual values of the active power, inactive power and neutral point potential deviation.

$$J=K_P|P^*(k+1)-P(k+1)|+K_Q|Q^*(k+1)-Q(k+1)|+K_o|u_o(k+1)|+K_sP_s(k+1) \quad (18)$$

The K_P, K_Q, K_o and K_s are the weight coefficients of the active power, inactive power, neutral point potential deviation and mean loss, respectively; $P^*(k+1)$ and $Q^*(k+1)$ are the pre-set values of the active power and inactive power of the system, respectively. The four weighting coefficients determine the importance of the target in the target cost function.

By configuring different weight coefficients, different control effects can be obtained. The weighting method is the most simple and effective multi-objective optimization method, which takes the optimal value function as the optimization index and ensures the uniqueness of the optimal solution. However, the disadvantages of this method are also obvious. The control effect depends on the selection of weight coefficient.

With the increase of optimization indexes, it is difficult to configure a single weight coefficient to accurately describe the desired effect. In addition, considering the conflict of various indexes, when one index of grid-connected inverter system is over-optimized, the control quality of the remaining indexes will deteriorate.

D. SELECTION OF WEIGHT COEFFICIENTS

In order to alleviate the conflict between different indexes and realize the global optimization that that takes the interests of all indexes into account, this paper designs the value function based on the satisfactory optimization method. Different from the traditional optimal control theory, satisfactory optimization does not seek the optimization of a single index when dealing with the multi-objective optimization problem of complex systems, but aims to obtain the satisfaction after the coordination of multiple indexes.

TABLE 2. Priorities of control objective.

Index	Optimized Content	Priority
Constraint	Jump limit of dv/dt	high
Satisfaction	Given power tracking Neutral voltage balance	medium
Optimization	Switching frequency reduction Switching loss equilibrium	low

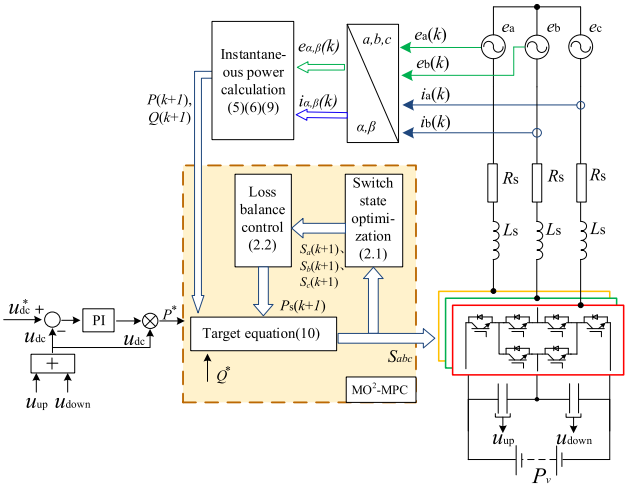

FIGURE 8. The block diagram on the MO²-MPC of three-level ANPC grid-connected inverter.

Considering the difference in importance of each optimization index of the three-level grid-connected inverters, its priority is divided as shown in Tab.2. At this point, the system optimization index is divided into high, medium and low priority.

The high priority is the system hard constraints of the system. Once the high priority index which plays a global role in the whole optimization process is broken, it will threaten the safe operation of the system. The medium priority index is the main control index. In the optimization process, objective satisfaction replaces the optimal one, in exchange for more control freedom, so that lower priority control targets participate in the optimization process. The low priority index is the auxiliary control index. When the optimization reaches low priority, if there are still more control degrees of freedom, then the influence of high and medium priority is ignored and the final output of the system is determined by the optimal low priority index to ensure the uniqueness of the whole optimization solution.

Based on the above control method, the block diagram on the MO²-MPC of three-level ANPC grid-connected inverter is shown as Fig.8.

Fig.9 is a flow chart of the MO²-MPC algorithm for a three-level ANPC grid-connected inverter, mainly includes the following 5 steps:

(1) According to the switching states $(S_a^{k-1}, S_b^{k-1}, S_c^{k-1})$ of the PWM rectifier according to the period of k-1,

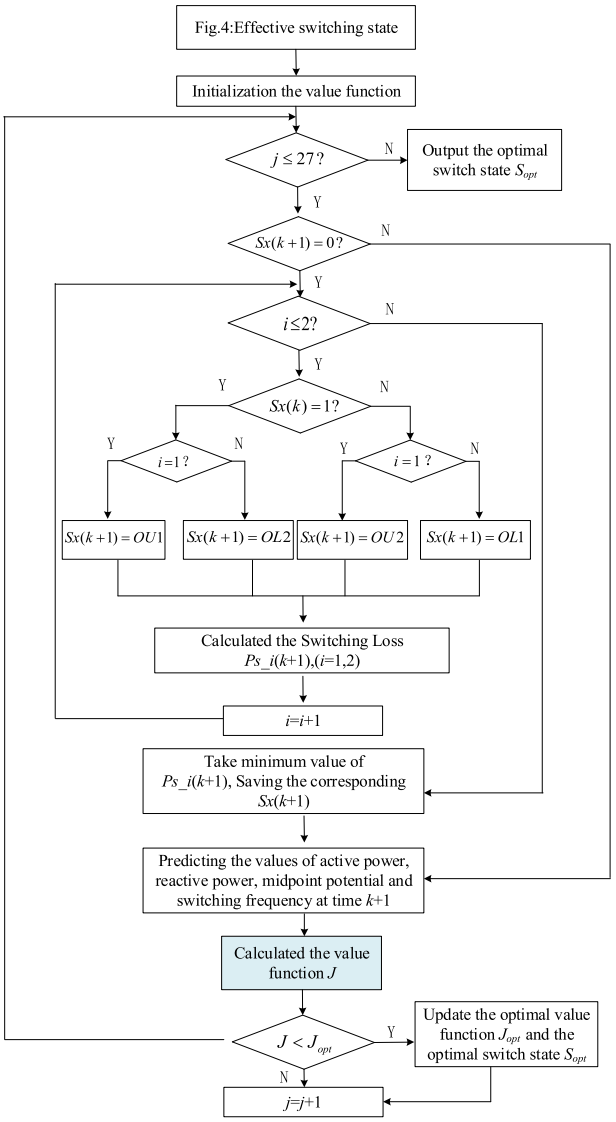

FIGURE 9. The flow chart of the MO^2-MPC algorithm for a three-level ANPC grid-connected inverter.

combined with Fig.4, all feasible switching states satisfying the switching jump constraint are determined;

(2) According to formula (7), formula (16) and formula (17), the grid side power, midpoint potential and switching loss of the $k+1$ time PWM rectifier corresponding to all feasible switching states are respectively predicted. Thereby getting $P(k+1)$, $Q(k+1)$, $u_o(k+1)$ and $P_s(k+1)$.

(3) The predicted values and the expected values of the system at time $k+1$ are substituted into the cost function formula (18), and the cost function corresponding to the feasible switch state is solved.

(4) The value of the cost function $\boldsymbol{J}$ corresponding to each switch state is compared one by one, and the switching state of the minimum cost function is obtained by comparison. The above switch state is the MO^2-MPC optimal solution.

(5) Finally, the switch state corresponding to the optimal solution is applied as the optimal switch state to the actual PWM rectification system.

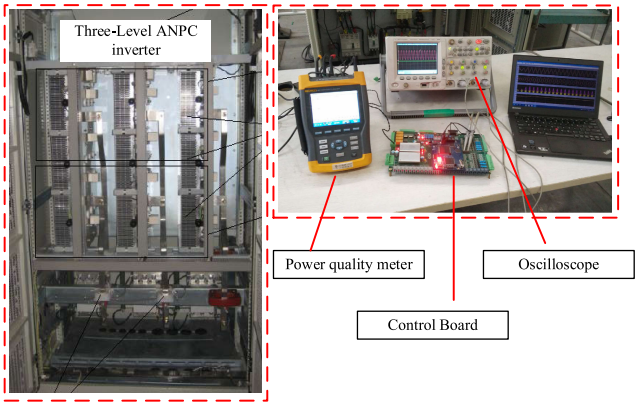

FIGURE 10. Photograph of the experiment equipments.

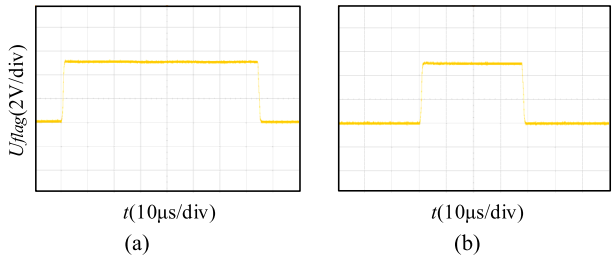

FIGURE 11. The maximum time required for rolling optimization of the processor. (a) Before optimization. (b) After optimization.

IV. EXPERIMENTAL VERIFICATION

The proposed control algorithm is verified through simulation on Matlab and experiment on a proto-type of three-level ANPC grid-connected inverter. The three-level ANPC grid-connected inverter experimental prototype was shown in Fig.10. The following parameters were used in the simulation and experiment: the effective value of AC-side line voltage of 260 V, the AC side frequency of 50 Hz, the reactance of 1.5 mH, the AC-side upper/lower bus capacitance of 4,000 μF, the pre-set DC voltage of 450 V, and the sampling interval of $T_s = 0.1$ ms. In the experiment, a pure resistive load of 16 Ω is applied to simulate the step load.

Fig.11 shows the maximum time required for rolling optimization of the processor before and after optimization. The waveform shows that the processor consumed 75 μs in calculation before the optimization, and 39 μs after the optimization. The runtime of the processor is shortened by nearly half, which agrees well with the theoretical analysis.

Fig.12 presents the waveforms of DC bus voltage, grid-side voltage and current and phase A port voltage measured in the steady state of MO^2-MPC. Judging by the waveform, the fluctuation of the DC side voltage is very small, and the fluctuation amplitude is within 5%, which satisfies the requirements of the general industry for DC voltage fluctuation. The grid-side voltage and current had phase coherence and the current was highly sinusoidal, posing little pollution to the grid; the phase A port voltage had no high-level jump. By analyzing the phase voltage waveform of phase A, it can be seen that the switching action of phase A in a power frequency cycle (20 ms) is about 16 times, and the corresponding

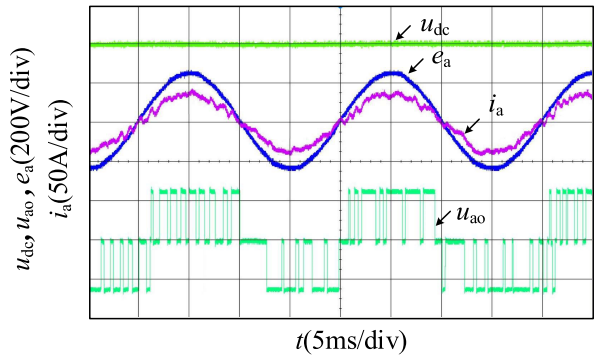

FIGURE 12. Experimental waveforms of related voltages and currents in the steady state of MO^2-MPC.

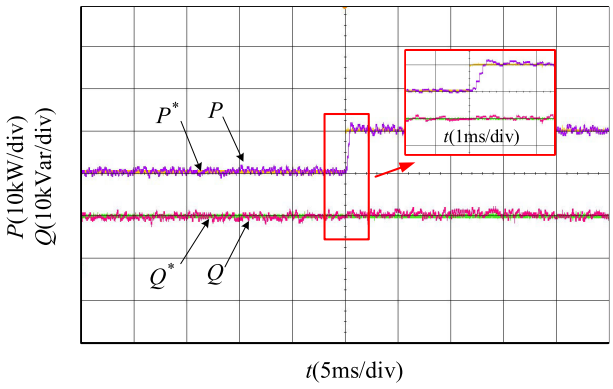

FIGURE 13. Experimental waveforms in the MO^2-MPC dynamic experiment.

switching frequency is about 800 Hz. The lower switching frequency means lower switching loss, so this control strategy is very suitable for high power converter control systems.

Fig.13 gives the waveforms recorded in the MO^2-MPC dynamic experiment. The waveforms show that, when the load changes suddenly, the active power follows the given power signal rapidly, and the response speed is within 1ms, while the reactive power is almost unchanged, which reflects that MO^2-MPC not only has fast dynamic performance but also achieves complete decoupling of active and reactive power. This means the control algorithm can make fast dynamic responses.

Fig.14 provides the spectrum waveform of the grid-side current harmonics of the grid-connected inverter in the conventional FCS-MPC and MO^2-MPC strategies. It can be seen from the waveform that the total harmonic distortion of the current dropped from 4.6% to 3.3%, which satisfies the relevant national standards in China. Hence, the proposed MO^2-MPC strategy can ensure the waveform quality of the load current.

Fig.15 (a) and (b) show the voltage waveforms of the DC-link capacitors in the conventional FCS-MPC and MO^2-MPC strategies, respectively. It can be seen from the figure that although the multi-target optimization control reduces the speed of the midpoint potential adjustment, the fluctuation amplitude of the two is almost the same from the fluctuation amplitude. Therefore, it can be concluded

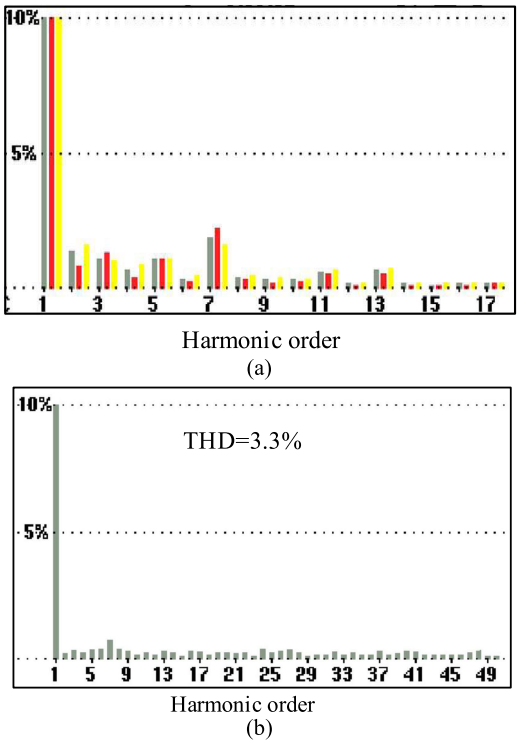

FIGURE 14. The spectrum diagram of grid-side current harmonics. (a) In the conventional FCS-MPC strategies. (b) In the conventional MO^2-MPC strategies.

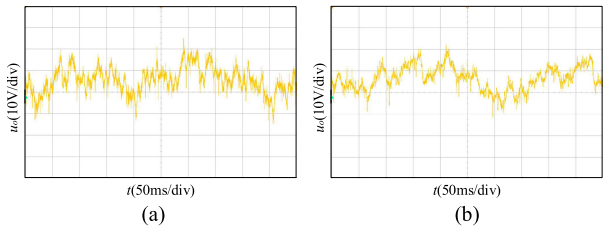

FIGURE 15. Waveforms of DC-link capacitor voltages. (a) In the conventional FCS-MPC strategies. (b) In the conventional MO^2-MPC strategies.

that although the multi-objective optimization control algorithm takes into considers of the multiple control objectives, the control accuracy of each single control target is not affected.

Fig.16 illustrates the power losses distribution of three-level NPC grid-connected inverter and ANPC inverter, under different power factors. The comparisons between the two figures show that the loss of power switches 1 and 4 is higher than other power switches in both types of three-level grid-connected inverters when the power factor was -1. However, the loss of power switches 1 and 4 in three-level NPC grid-connected inverter is nearly twice as much as that of the corresponding power switches in three-level ANPC grid-connected inverter. Moreover, the loss of power switches 1 and 4 started to move to power switches 2 and 3, with the increase of the power factor. These results show that the clamping power switches can effectively balance the loss of other power switches in three-level ANPC grid-connected

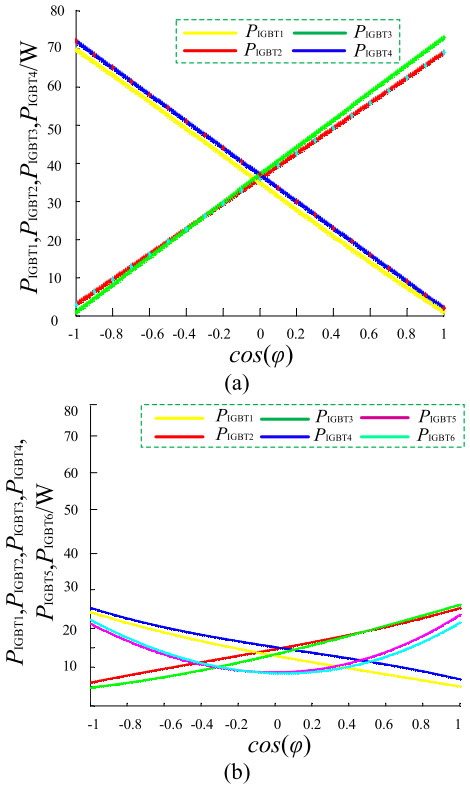

FIGURE 16. Power loss waveforms under different power factors. (a) The waveform of three-level NPC grid-connected inverter. (b) The waveform of three-level ANPC grid-connected inverter.

inverter, and thus strike a balance between all power switches in power loss. This further proves that the proposed control strategy can achieve the control target of balancing the loss of power switches.

Fig.17 are the temperature rise cloud maps of IGBTs on a bridge arm in the three-level ANPC grid-connected inverter before and after optimization under the rated power factor. Comparing the two figures, it can be seen that the overall temperature rise of the system was relatively high before the optimization, and mainly concentrated on IGBT2 and IGBT3. The temperature of the IGBTs peaked at 77°. After the inverter was optimized by the proposed MO^2-MPC algorithm, the highest temperature of the IGBTs was only 60°, because the algorithm balanced the switching losses of power switches and evened out the temperatures on these power switches. The comparison verifies the correctness and effectiveness of the proposed algorithm.

Fig.18 shows the temperture bar graph of IGBTs on a bridge arm of the ANPC grid-connected inverter. Blue and red bars respectively represent the average temperature wavefoms of each switch tube of the ANPC three-level grid-connected inverter in steady state without or with the control strategy proposed in this paper. Compared with the traditional strategy, the MO^2-MPC control algorithm can effectively balance the loss of each switch tube in the bridge arm, so as to enhance the maximum output power of the device.

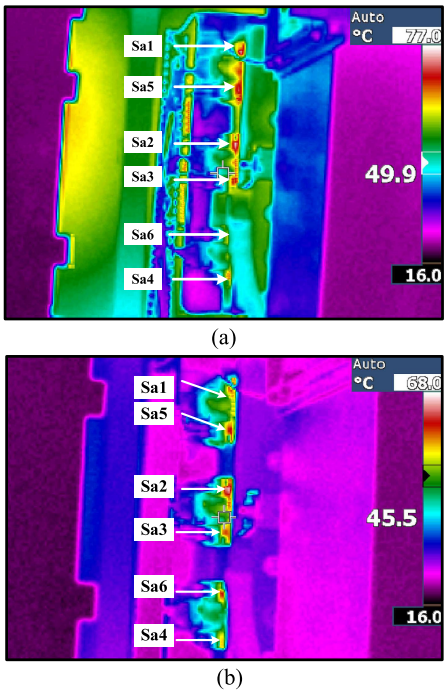

FIGURE 17. The temperature rise cloud maps of IGBTs on a bridge arm in the three-level ANPC grid-connected inverter. (a) Before the optimization. (b) After the optimization.

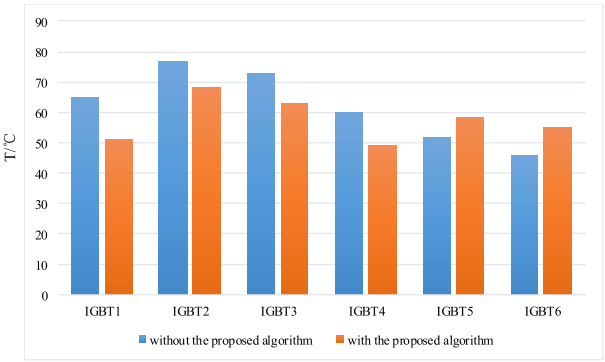

FIGURE 18. The temperature column graph of IGBTs on a bridge arm in the three-level ANPC grid-connected inverter.

V. CONCLUSION

This paper proposes and analyzes the MO^2-MPC principles for three-level ANPC grid-connected inverter and details the way to implement the MO^2-MPC algorithm. This control strategy can effectively reduce the number of rolling optimizations in the MPC, dramatically shorten the runtime of the processor, and realize unit power factor control of three-level grid-connected inverter, giving the system excellent dynamic and static performances. Besides, the switch tube losses of three-level ANPC grid-connected inverter were modeled, the power loss balance equation for power switch tubes is derived, and the proposed control method is verified through experiments. The results show that the control method achieved the expected effect, indicating that the proposed control algorithm is correct.

REFERENCES

[1] K. M. Abughalieh and S. G. Alawneh, "A survey of parallel implementations for model predictive control," *IEEE Access*, vol. 7, pp. 34348–34360, 2019.
[2] B. Zhao, X. Wang, D. Lin, M. M. Calvin, J. C. Morgan, R. Qin, and C. Wang, "Energy management of multiple microgrids based on a system of systems architecture," *IEEE Trans. Power Syst.*, vol. 33, no. 6, pp. 6410–6421, Nov. 2018.
[3] P. Hyatt and M. D. Killpack, "Real-time nonlinear model predictive control of robots using a graphics processing unit," *IEEE Robot. Autom. Lett.*, vol. 5, no. 2, pp. 1468–1475, Apr. 2020.
[4] A.-H. Mohsenian-Rad, V. W. S. Wong, J. Jatskevich, R. Schober, and A. Leon-Garcia, "Autonomous demand-side management based on game-theoretic energy consumption scheduling for the future smart grid," *IEEE Trans. Smart Grid*, vol. 1, no. 3, pp. 320–331, Dec. 2010.
[5] A. Ghosal and M. Conti, "Key management systems for smart grid advanced metering infrastructure: A survey," *IEEE Commun. Surveys Tuts.*, vol. 21, no. 3, pp. 2831–2848, 3rd Quart., 2019.
[6] M. Benmalek, Y. Challal, A. Derhab, and A. Bouabdallah, "VerSAMI: Versatile and scalable key management for smart grid AMI systems," *Comput. Netw.*, vol. 132, pp. 161–179, Feb. 2018.
[7] K. Sharma and L. Mohan Saini, "Performance analysis of smart metering for smart grid: An overview," *Renew. Sustain. Energy Rev.*, vol. 49, pp. 720–735, Sep. 2015.
[8] M. Kuzlu, M. Pipattanasomporn, and S. Rahman, "Communication network requirements for major smart grid applications in HAN, NAN and WAN," *Comput. Netw.*, vol. 67, pp. 74–88, Jul. 2014.
[9] T. Wang, D. O'Neill, and H. Kamath, "Dynamic control and optimization of distributed energy resources in a microgrid," *IEEE Trans. Smart Grid*, vol. 6, no. 6, pp. 2884–2894, Nov. 2015.
[10] D. Christen and J. Biela, "Analytical switching loss modeling based on datasheet parameters for MOSFETs in a half-bridge," *IEEE Trans. Power Electron.*, vol. 34, no. 4, pp. 3700–3710, Apr. 2019.
[11] Y. Jiao and F. C. Lee, "New modulation scheme for three-level active Neutral-Point-Clamped converter with loss and stress reduction," *IEEE Trans. Ind. Electron.*, vol. 62, no. 9, pp. 5468–5479, Sep. 2015.
[12] R. Vargas, P. Cortes, U. Ammann, J. Rodriguez, and J. Pontt, "Predictive control of a three-phase Neutral-Point-Clamped inverter," *IEEE Trans. Ind. Electron.*, vol. 54, no. 5, pp. 2697–2705, Oct. 2007.
[13] M. Aguirre, S. Kouro, C. A. Rojas, J. Rodriguez, and J. I. Leon, "Switching frequency regulation for FCS-MPC based on a period control approach," *IEEE Trans. Ind. Electron.*, vol. 65, no. 7, pp. 5764–5773, Jul. 2018.
[14] L. Grüne and M, Stieler, "Multiobjective model predictive control for stabilizing cost criteria," *Discrete Continuous Dyn. Syst. B*, vol. 24, no. 8, pp. 3905–3928, Aug. 2019.
[15] J. D. Barros, J. F. A. Silva, and E. G. A. Jesus, "Fast-predictive optimal control of NPC multilevel converters," *IEEE Trans. Ind. Electron.*, vol. 60, no. 2, pp. 619–627, Feb. 2013.
[16] T. J. Vyncke, S. Thielemans, and J. A. Melkebeek, "Finite-set model-based predictive control for flying-capacitor converters: Cost function design and efficient FPGA implementation," *IEEE Trans Ind. Informat.*, vol. 9, no. 2, pp. 1113–1121, May 2013.
[17] Y. Luo and C. Liu, "A simplified model predictive control for a dual three-phase PMSM with reduced harmonic currents," *IEEE Trans. Ind. Electron.*, vol. 65, no. 11, pp. 9079–9089, Nov. 2018.
[18] M. J. Navardi, J. Milimonfared, and H. A. Talebi, "Torque and flux ripples minimization of permanent magnet synchronous motor by a predictive-based hybrid direct torque control," *IEEE J. Emerg. Sel. Topics Power Electron.*, vol. 6, no. 4, pp. 1662–1670, Dec. 2018.
[19] Y. Deng, J. Li, K. H. Shin, T. Viitanen, M. Saeedifard, and R. G. Harley, "Improved modulation scheme for loss balancing of three-level active NPC converters," *IEEE Trans. Power Electron.*, vol. 32, no. 4, pp. 2521–2532, Apr. 2017.
[20] T. Bruckner, S. Bernet, and H. Guldner, "The active NPC converter and its loss-balancing control," *IEEE Trans. Ind. Electron.*, vol. 52, no. 3, pp. 855–868, Jun. 2005.
[21] C. H. Huang and C. Ch Chen, "A high-efficiency current-mode buck converter with a power-loss-aware switch-on-demand modulation technique for multifunction SoCs," *IEEE Trans. Power Electron.*, vol. 31, no. 12, pp. 8303–8316, 2016.
[22] M. Rodríguez, A. Rodríguez, P. F. Miaja, D. G. Lamar, and J. S. Zúniga, "An insight into the switching process of power MOSFETs: An improved analytical losses model," *IEEE Trans. Power Electron.*, vol. 25, no. 6, pp. 1626–1640, Jun. 2010.
[23] J.-W. Yang and H.-L. Do, "Efficient single-switch Boost-Dual-Input flyback PFC converter with reduced switching loss," *IEEE Trans. Ind. Electron.*, vol. 62, no. 12, pp. 7460–7468, Dec. 2015.

ZHENGLONG XIA (Member, IEEE) received the B.S. degree in electrical engineering and automation, the M.S. degree in power system and automation, and the Ph.D. degree in power electronics and power drives from the China University of Mining and Technology, in 2005, 2008 and 2014, respectively. Since 2014, he has been an Associate Professor with the Department of Electrical Engineering and Automation, Jiangsu Normal University, China, where he is responsible for youth fund of the Foundation Research Project of Jiangsu Province. Since 2019, he has been a Visiting Scholar with Aalborg University, Denmark. He has published more than 40 journal articles in the fields of power quality management and fault diagnosis. His research interests are reactive compensation of power systems, fault diagnosis, and circuit theory and systems.

ZHAN LIU (Member, IEEE) received the B.S. degree in electrical engineering and automation, the M.S. degree in power electronics and power drives, and the Ph.D. degree in electrical engineering from the China University of Mining and Technology, Xuzhou, Jiangsu, China, in 2011, 2013 and 2016, respectively. Since 2017, he has been a university Lecturer with the Department of Electrical Engineering and Automation, Jiangsu Normal University, China, where he is responsible for a National Natural Science Foundation of China.

His research interests include power electronics, modern control theory, model predictive control, and multilevel converter.

JOSEP M. GUERRERO (Fellow, IEEE) received the B.S. degree in telecommunications engineering, the M.S. degree in electronics engineering, and the Ph.D. degree in power electronics from the Technical University of Catalonia, Barcelona, in 1997, 2000, and 2003, respectively. Since 2011, he has been a Full Professor with the Department of Energy Technology, Aalborg University, Denmark, where he is responsible for the Microgrid Research Program. Since 2014, he has been the Chair Professor with Shandong University; since 2015, he has been a Distinguished Guest Professor with Hunan University; and since 2016, he has been a Visiting Professor Fellow with Aston University, U.K., and a Guest Professor with the Nanjing University of Posts and Telecommunications. Since 2019, he became a Villum Investigator by The Villum Foundation, which supports the Centre for Research on Microgrids (CROM), Aalborg University, being the Founder and Director of CROM. He has published more than 500 journal articles in the fields of microgrids and renewable energy systems, which are cited more than 30,000 times. His research interests are oriented to different microgrid aspects, including power electronics, distributed energy-storage systems, hierarchical and cooperative control, energy management systems, smart metering, and the Internet of Things for AC/DC microgrid clusters and islanded minigrids. Specially focused on maritime microgrids for electrical ships, vessels, ferries, and seaports.

Dr. Guerrero was elevated as an IEEE Fellow for his contributions on distributed power systems and microgrids, in 2015. He received the Best Paper Award of the IEEE TRANSACTIONS ON ENERGY CONVERSION for the period 2014–2015 and the Best Paper Prize of the IEEE Power and Energy Society, in 2015. He also received the Best Paper Award of *Journal of Power Electronics*, in 2016. During five consecutive years, from 2014 to 2018, he was awarded by Clarivate Analytics (former Thomson Reuters) as Highly Cited Researcher. He is an Associate Editor for a number of the IEEE Transactions.